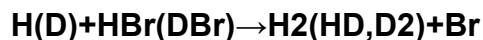


Reactive cross section as a function of reagent energy. II.



J. W. Hepburn, D. Klimek, K. Liu, R. G. Macdonald, F. J. Northrup, and J. C. Polanyi

Citation: *The Journal of Chemical Physics* **74**, 6226 (1981); doi: 10.1063/1.441014

View online: <http://dx.doi.org/10.1063/1.441014>

View Table of Contents: <http://scitation.aip.org/content/aip/journal/jcp/74/11?ver=pdfcov>

Published by the **AIP Publishing**

Articles you may be interested in

[Experimental determination of total reactive cross sections for \$H+D_2\(v=0\)\rightarrow HD+D\$ at \$E_{c.m.}=2.11\$ and \$1.54\$ eV](#)
J. Chem. Phys. **86**, 3047 (1987); 10.1063/1.452752

[Total reactive cross sections for the reaction \$H+D_2=HD+D\$](#)
J. Chem. Phys. **84**, 1934 (1986); 10.1063/1.450444

[Effect of J dependence of Raman cross sections on CARS product quantum state distributions for the \$H+D_2\rightarrow HD+D\$ reaction](#)
J. Chem. Phys. **83**, 1605 (1985); 10.1063/1.449397

[Experimental study of the dynamics of the \$H+D_2\rightarrow HD+D\$ reaction at collision energies of 0.55 and 1.30 eV](#)
J. Chem. Phys. **81**, 1298 (1984); 10.1063/1.447762

[Reactive cross section as a function of collision energy. I. \$H\(D\)+Br_2\rightarrow HBr\(DBr\)+Br\$](#)
J. Chem. Phys. **69**, 4311 (1978); 10.1063/1.437088



Reactive cross section as a function of reagent energy. II. $\text{H(D)} + \text{HBr(DBr)} \rightarrow \text{H}_2(\text{HD, D}_2) + \text{Br}$

J. W. Hepburn,^{a)} D. Klimek,^{b)} K. Liu,^{c)} R. G. Macdonald,^{d)} F. J. Northrup, and J. C. Polanyi

Department of Chemistry, University of Toronto, Toronto, Canada M5S 1A1
(Received 29 December 1980; accepted 20 February 1981)

A crossed molecular beam study has been made of reactive cross section as a function of collision energy $S_r(E_T)$ for all isotopic variants of the abstraction reaction $\text{H}' + \text{H}''\text{Br} \rightarrow \text{H}'\text{H}'' + \text{Br}$. The apparatus incorporates, for reagent preparation, a supersonic source of variable-energy H or D atoms, and, for product detection, a tunable vacuum ultraviolet laser to obtain laser-induced fluorescence of Br. The cross-section functions indicate that the threshold energy for reaction is < 1 kcal/mol. At enhanced collision energy of $E_T = 7$ kcal/mol, the observed order of reactivity in the isotopic series designated (H', H'') was $(\text{D, H}) \geq (\text{D, D}) > (\text{H, H}) > (\text{H, D})$. As noted in a previous report from this laboratory [Int. J. Chem. Kinet., Laidler Festschrift (in press)] the favorable kinematics for (D, H) as compared with (H, D) can be understood in terms of lengthened interaction time for D atom reaction (compared with H) and diminution in the time required for HBr (compared with DBr) to rotate into the preferred alignment for reaction. The effect is illustrated here in terms of a simple model of reaction. The experimental data obtained in this work at low collision energy, in conjunction with 300 K rate constants obtained by others, suggest that close to threshold, kinematic effects are supplanted by threshold effects, yielding $S_r(\text{H, D}) > S_r(\text{D, H})$, the inverse of the principal isotope effect at enhanced collision energy.

I. INTRODUCTION

One of the major advances towards the as yet unattained experimental goal of "state-to-state chemistry" has been the combination of molecular beams with laser-induced fluorescence product detection.^{1,2} The recent use of supersonic beams in laser-induced fluorescence (LIF) experiments has enabled product internal energy distributions to be determined at specified reagent collision energies.³ In this paper we shall discuss the extension of the laser-induced fluorescence technique into a new spectral region below 2000 Å (the vacuum ultraviolet or VUV).

In our laboratory we have combined a recently developed, widely tunable VUV laser with a crossed molecular beam apparatus employing supersonic atomic beams, in order to carry out chemical dynamics studies. This apparatus will be described in some detail in the experimental section of this paper. The variable energy supersonic atomic hydrogen beam source used in the experiments reported here and previously⁴ will also be described in detail for the first time.

In the present paper we have applied this apparatus to the study of "abstraction" reactions $\text{H}' + \text{H}''\text{Br} \rightarrow \text{H}'\text{H}'' + \text{Br}$. The product Br atom was detected by LIF at the 1541 Å resonance line of Br.⁵

The reactions studied in the present experiments were



This family of reactions has been the subject of recent studies under thermal conditions by Endo and Glass,⁶ and also by Husain and Slater.⁷ We shall compare these thermal data with our low collision-energy data in Sec. IV C of this paper. Endo and Glass were also able to measure the rate constant for the alternative reaction pathway $\text{H}' + \text{H}''\text{Br} \rightarrow \text{H}'\text{Br} + \text{H}''$ (termed "exchange").

Nonthermal studies of these reactions have been made using as reagent H or D recoiling from photolytically dissociated HI or DI.^{8,9} Under 300 K thermal conditions, for X = Br, the abstraction reaction was found to be substantially faster than exchange⁸; however, the reverse was the case at enhanced reagent collision energy.

Previous molecular beam experiments dealt with the exchange process at enhanced collision energy: $\text{H}' + \text{H}''\text{X} \rightarrow \text{H}'\text{X} + \text{H}''$ (X = Cl, Br, I).^{10,11} The present study relates exclusively to the abstraction pathway. It also differs from earlier beam studies employing H or D¹² as reagent (with the atoms coming from an effusive source at 2800 K) in using a supersonic source of H or D so that the collision energy was systematically variable.

Isotope effects seen in reactions involving hydrogen atoms provide a test for theories of reaction rates, since substantial changes in the rate of reaction occur without a change in the potential energy surface on which the reaction takes place.¹³ In the abstraction reactions studied here both the attacking atom and the atom exchanged are hydrogen, resulting in the possibil-

^{a)} Present address: Lawrence Berkeley Laboratories, University of California, Berkeley, Cal. 94720.

^{b)} Present address: AVCO Everett Research Laboratory, Inc., 2385 Revere Beach Parkway, Everett, Mass. 02149.

^{c)} Present address: Atmospheric Science Division, School of Geophysical Science, Georgia Institute of Technology, Atlanta, Ga. 30332.

^{d)} Present address: Physical Chemistry Branch, Atomic Energy of Canada Ltd., Chalk River Nuclear Laboratories, Chalk River, Ontario K0J 1J0.

ity of varied changes in the reaction rate down the series.

The use of a supersonic H and D atom source in the present experiments allows us to study the cross sections for the abstraction reactions (1)–(4) at defined collision energies E_T . The behavior of these cross sections $S_r(E_T)$ gives an indication of the magnitude of the translational energy barrier for reaction on the $H'H''Br$ surface.

The isotope effects found in this work show an interesting kinematic effect at higher E_T . This effect is attributed to alignment of the reaction intermediate into a preferred configuration in the course of the reactive collision. Such behavior has been noted previously in theoretical studies,^{14–16} but this is the first experimental evidence for this effect. A simple model is used to describe the effect that this alignment will have on the reactive cross section for $A + BC$ reactions.

In what follows, the reactions (1)–(4) will be referred to using the notation (H', H'') , where H' and H'' are either H or D, and H' refers to the attacking atom and H'' to the atom being transferred [e.g., Reaction (2) will be referred to as (H, D)].

II. EXPERIMENTAL

A. General machine description

The basic machine used in these experiments is shown in Fig. 1. A major advantage of this apparatus was the large pumping speed in the source and scattering chambers. In the source chamber, in particular, the use of a 16 in. booster pump, with its high mass throughput, allowed the use of very high intensity supersonic beams. The pump used was an unbaffled Stokes 16 in. ring jet booster pump (series 150), with a pumping speed of 4500 ℓ/s at 10^{-2} Torr. This was backed

by a 150 ft^3/min Stokes Microvac mechanical pump. With this high pumping speed and pressure tolerance, flows as high as 2×10^{-3} mol/s could be used, which gave a source chamber pressure of 8×10^{-3} Torr. These flows are an order-of-magnitude larger than those usually used in molecular beam systems; they correspond to 5 atm of nitrogen at 300 K behind a 300 μ orifice.

The supersonic source was located about 15 mm behind a 2 mm skimmer, and about 10 cm from the center of the reaction zone. The skimmed supersonic beam crossed the main (scattering) chamber, which was 1 m in diameter and was pumped by a baffled 32 in. NRC HS diffusion pump. The baffle was a home-built chevron baffle cooled by a Freon refrigerator. Its normal operating temperature was -30°C . The diffusion pump was backed by a 150 cfm Stokes microvac pump, and the measured pumping speed in the main chamber was 12 000 ℓ/s at 10^{-4} Torr. The normal operating pressure of this chamber with both beams on was in the mid- 10^{-5} Torr range.

The supersonic beam was crossed at 90° by an effusive molecular beam from a multicapillary array source. The vacuum ultraviolet (VUV) probe laser passed through the center of this reaction volume. A solar blind photomultiplier (PMT 1) was suspended above the reaction zone, and a LiF lens was used to collect the fluorescence and collimate it onto the photocathode. The VUV laser intensity was monitored by a second photomultiplier (PMT 2).

The atomic beam was modulated in the main chamber before it entered the mass spectrometer chamber. The collimating orifice on this latter chamber was 5 mm in diameter and 16 cm ahead of the mass spectrometer ionizer. This final chamber was pumped by a liquid nitrogen baffled 6 in. VHS diffusion pump. The operating pressure was in the 10^{-7} Torr range.

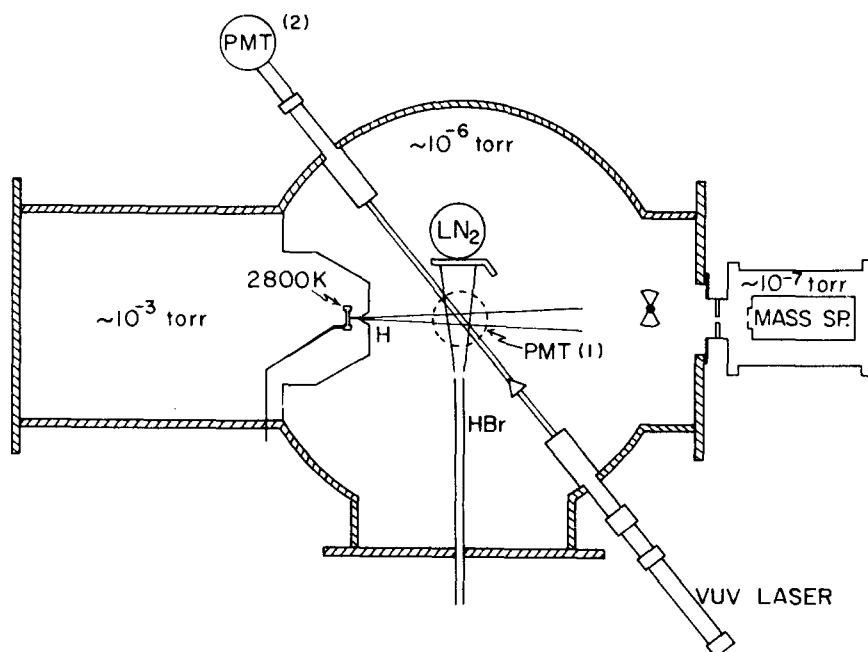


FIG. 1. Schematic diagram of the molecular beam apparatus for the $H' + H''Br$ experiments, viewed from the top of the machine. The source chamber is at the left, followed by the main (scattering) chamber and the mass spectrometer chamber.

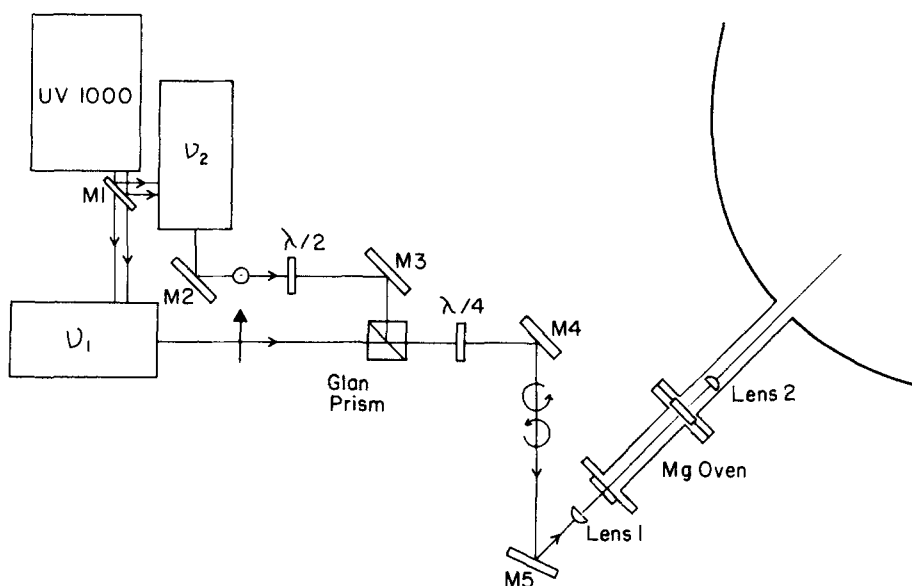


FIG. 2. Schematic diagram of the optical setup for the four-wave mixing. The UV-1000 N_2 laser is made by Moleclectron. It pumps two dye lasers, labeled ν_1 and ν_2 . The two dye lasers are combined in an air space glan-laser prism as shown. Polarizations of the dye lasers are indicated by the arrows on the laser beams. The $\frac{1}{4}$ wave and $\frac{1}{2}$ wave plates are marked $\lambda/4$ and $\lambda/2$, respectively. M1 is a 50% beamsplitter, and M2 to M5 are 100% reflective mirrors. Lens 1 is a 20 cm achromat, and lens 2 is a 20 cm LiF planoconvex lens. The main chamber of the molecular beam apparatus is at the right.

B. Vacuum ultraviolet laser

Pulsed dye lasers are capable of producing tunable radiation from the near UV to the near IR, depending on the pump wavelength. To produce a tunable laser in other regions of the spectrum, use is made of some form of frequency mixing in a nonlinear material. The properties of these materials are such that they respond in a nonlinear fashion to an applied electric field, and thus can oscillate at frequencies that are sums and differences of the input frequencies.¹⁷

To get to $< 2000 \text{ \AA}$ by frequency mixing, the best method is four-wave sum mixing in vapors. There are several methods of doing this.^{18,19} One of the most efficient is resonantly enhanced four-wave mixing in metal vapors.²⁰ The nonlinear medium used in the present study to generate VUV in the 1400–1600 \AA region was Mg vapor, phase matched with He, as first described by Wallace and Zdasiuk.²¹ The laser setup was essentially a copy of their prototype laser, with a few modifications. The experimental arrangement and theory of operation have been described elsewhere,²² and only an outline will be given here.

The VUV laser is shown schematically in Fig. 2. A Moleclectron UV-1000 nitrogen laser pumped two home-built Hänsch-type dye lasers.²³ These dye lasers produced a pulse of 5 ns duration with 30 kW peak power. The measured bandwidth was $0.2\text{--}0.3 \text{ cm}^{-1}$ (the single shot bandwidth was 0.1 cm^{-1} , but vibrations caused a small frequency jitter). The two dye lasers were combined in a glan-laser prism and were focused into the Mg vapor oven by a 20 cm achromat lens. The VUV output was recollimated by a 20 cm LiF lens after the Mg oven.

The Mg vapor oven consisted of a replaceable 1 in. diameter stainless steel tube with 0.25 in. copper tubing soldered onto each end for water cooling. This 11 in. long tube was held between two window-mounting assemblies by O-ring compression vacuum seals. Inside the tube was a wick, consisting of three layers

of fine nickel mesh interspersed with three layers of fine stainless steel mesh, such that the stainless mesh formed the innermost layer.

The oven was heated by three 2 in. long, 240 W cylindrical heaters, which surrounded the central part of the tube. The oven temperature was monitored by three thermocouples clamped to the outside of the tube. In normal operation, only the central heater was used. The two side heaters were only required for melting Mg crystals.

For an experiment, the oven was filled with 150 Torr of He gas and the central heater was maintained at a temperature of 750°C . The vapor pressure of Mg in the oven was 15 Torr at this temperature. With a new central tube, the oven could be used for 12–16 h continuously before Mg crystals blocked the optical path. When this became a problem, the central heater was turned off and full power was applied to the two end heaters until the Mg crystals melted. The end heaters were then turned off, and the central heater turned back on. By means of this cycling method the oven could be used continuously for long periods of time. A further gram of Mg metal was added to the oven before each subsequent run. When crystals formed beyond the end heaters, or when the time between cycling dropped to a few hours, the central tube was changed.

With the oven at operating temperature, and the ν_2 laser blocked, the third harmonic signal ($3\nu_1$) was maximized. It was then suppressed by inserting a quarter-wave plate into the laser path after the glan prism. At this point ν_2 was unblocked and the overlap optimized by maximizing the VUV intensity. With good overlap, this tunable output ($2\nu_1 + \nu_2$) had an intensity comparable to the $3\nu_1$ intensity.

The laser intensity was monitored by a solar blind PMT (EMI G26E314LF) as follows: After the VUV laser exited from the machine through the LiF exit window, it was spatially dispersed by a sand-blasted Cu elbow. A fraction of this dispersed light was de-

ected by the PMT. To prevent air absorption, the region between the exit window and the PMT was flushed with a slow flow of argon.

C. Laser induced fluorescence method

A schematic diagram of the LIF system is shown in Fig. 3. The recollimated laser beam was brought to the reaction zone through 20 cm of light baffles. These consisted of a series of discs, blackened with Nextel, with collimating holes in the center. These discs were about 1.5 cm apart, and the whole assembly was surrounded by a blackened sheath. The laser passed through the center of the scattering volume beyond these baffles. After this, the laser passed through an identical set of light baffles and exited through a LiF exit window and was monitored as described above.

The fluorescence from the products was collimated by an $f/1$ 3.8 cm focal length LiF lens located 4.5 cm above the laser. This lens formed the entrance window to a hermetically sealed PMT housing which was flushed by a slow flow of argon. 3 cm above the lens was an EMR 542-G-08-18 solar blind PMT with a 28 mm diameter CsI photocathode. The signal from this phototube (a current pulse of about 30 ns FWHM) was terminated into the 50 Ω input of an Ortec $\times 10$ fast preamplifier. The output from this preamp went either to a 100 MHz storage scope or to the boxcar for aver-

aging. The signal from the intensity monitor PMT was taken directly to the scope or boxcar, where it was terminated into 50 Ω .

The signal processing electronics were triggered by a photodiode looking at stray light from the dye lasers. The signal from the fluorescence monitor PMT (I_{SIG}) or from the intensity monitor PMT (I_{VUV}) could be viewed on the scope for initial alignment or wavelength tuning.

To average these signals, they were first put through delay lines (because of the 75 ns dead time of the boxcar) which consisted of 50 ft of 50 Ω BNC cable. The delayed signal pulses were then put into the signal inputs of a PAR 162 boxcar with two 164 plug ins. The signal pulses, with a 20 Hz repetition rate, were averaged over a 30 ns gate width and the output voltage of the boxcar, which was proportional to I_{SIG} and I_{VUV} , was recorded on a two-pen recorder.

D. Supersonic H and D atom source

These experiments required a controlled and variable collision energy as well as high flux of reagents. In order to achieve both of these aims under molecular beam conditions, a supersonic source must be used. In the present experiments, the atomic reagent was very much lighter than the molecular reagent, so the center-of-mass collision energy could be controlled by controlling the atomic velocity.

This involved construction of a supersonic atomic hydrogen source with variable collision energy, something not yet reported in the literature. In order to achieve the high pressures necessary for a supersonic source, thermal dissociation was used to generate the H or D atoms. As the temperature required to dissociate H_2 is extremely high (~ 2800 K), the energy of the beam could not be varied by varying the oven temperature. Instead, the seeding technique²⁴ was used to vary the atomic velocity, i.e., the H_2 or D_2 was diluted with inert gas and the mixture expanded out of an oven source. In the expansion the H or D atoms slowed down to the bulk gas velocity. To vary the atomic velocity, the diluent gas was changed.

In order to achieve the required temperatures, a resistively heated tungsten oven was used. This oven was similar in design to one used by Herschbach and co-workers²⁵ to make an effusive H atom beam. The W oven was custom fabricated by Ultramet Inc. and consisted of a 5 cm long vapor deposited W tube (4.06 mm o.d., 0.51 mm wall thickness) with 6.4 mm long, 6.4 mm o.d. copper sleeves brazed on both ends. A 0.2 mm (200 μ) hole was spark eroded in the center of the tube.

A stainless steel plug was silver soldered into one end of this oven. After careful cleaning, the gas feed was soldered onto the other end. The oven was then mounted in the copper electrode blocks, and the orifice was aligned. At this point the source assembly was ready for mounting in the machine.

The water cooling lines to the source assembly were

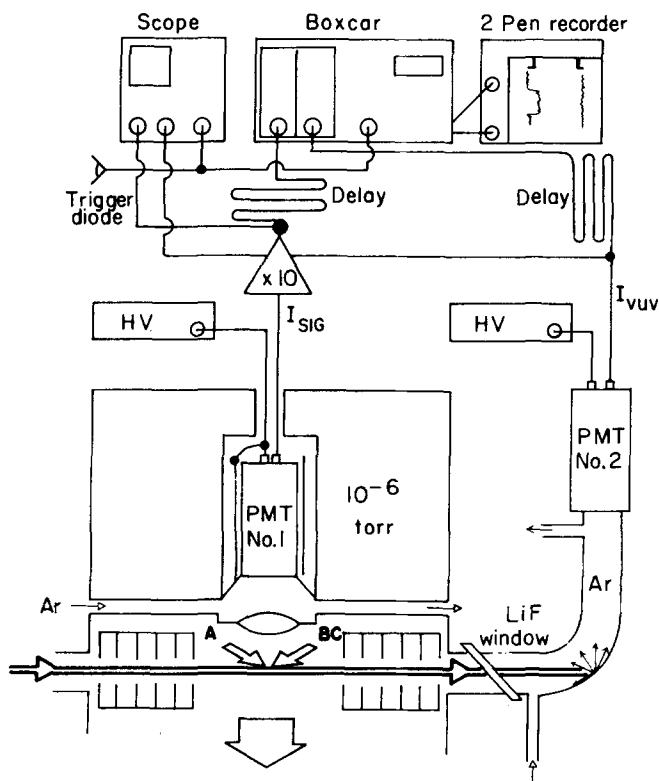


FIG. 3. Schematic diagram of the apparatus. Molecular beams are indicated by arrows marked "A" and "BC." The VUV probe laser is shown as an arrow passing through the beam crossing point. The 10^{-6} Torr chamber is the main chamber of Fig. 1.

also the electrical leads for the oven. The cooling lines were made from 0.25 in. copper tubing and a supply plus drain line was provided for each electrode clamp. To heat the oven, 7 V ac were passed through it, resulting in a current of 360 A. This voltage was supplied by a (home-built) 1000 A, 0 to 12 V ac power supply.

The source was mounted on an x - y - z translator so that the nozzle was about 15 mm behind a 2 mm nickel skimmer. The skimmer was able to withstand the extreme heat load on it without distortion or destruction of its edge. The x - y - z translator was used to vary the nozzle-skimmer distance and to optimize the nozzle-skimmer alignment while the source was at operating temperature.

The gas mixtures used for the seeded beams were made on line in a high pressure gas mixing system which supplied gas to the supersonic atomic beam source. High pressures of H_2 or D_2 and the diluent gas were put ahead of two fine metering needle valves, which fed gas through a mixing region and then into the source. These needle valves were adjusted to give the desired flow of H_2 or D_2 (as measured with a Haystings-Raydist mass flowmeter) as well as a known total pressure in the source oven. When the pressure had stabilized, the oven could run for several hours without further adjustment.

E. Beam characterization

In order to measure the density of H or D atoms in the reaction zone, the atomic density in the supersonic beam was monitored by mass spectrometry. The mass spectrometer used in these experiments was a high resolution quadrupole mass spectrometer with 19 mm diameter rods, made by Extranuclear Laboratories. This mass spectrometer had a high efficiency electron impact ionizer and used a Dumont 14 stage electron multiplier as the ion detector. The signal current from the electron multiplier was taken from the last dynode by a short shielded cable, and terminated on the outside of the chamber into 10–100 k Ω . After this, the resulting voltage was amplified by a PAR 115 pre-amplifier and detected by a phase sensitive amplifier or, in the case of the time of flight experiments, by a PAR model 162 boxcar integrator.

Because of the high pressures of hydrogen or deuterium used in the source oven, the degree of dissociation of H_2 or D_2 , i.e., α , in the source oven was fairly small, on the order of 1%. Thus, atomic H or D was only a minor component of the beam gas mixture. Because molecular H_2 or D_2 is present in a much higher concentration than atomic H or D, the contribution of dissociative ionization of the molecule to the atomic signal must be corrected for precisely.

The atomic density N_1 is related to the signals at the atomic and molecular masses S_1 and S_2 , respectively, by the simple relation

$$N_1 \propto S_1 - \delta S_2, \quad (5)$$

where δ is a constant related to the dissociative ioniza-

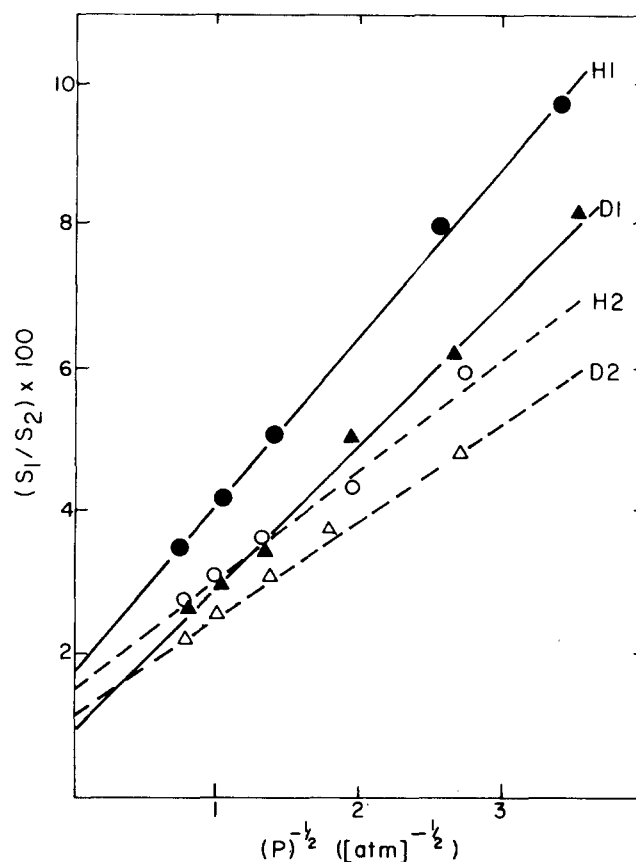


FIG. 4. Plots to determine R_1/R_2 and δ for H atoms, and R_2/R_1 and δ for D atoms. The data are given as points, with the least-squares lines drawn through them. Data are from two different experiments. Circles are for H, and triangles for D.

tion process.

Since δ can vary with temperature,²⁶ it must be defined at the source operating temperature. To do this, δ can be determined at several temperatures where α is insignificant (thus, $\delta = S_1/S_2$) and extrapolated to the operating temperature. Or, to avoid extrapolation, if α is small and the detectivities of the atomic and molecular species are comparable, then the following can be shown²⁷:

$$\frac{S_1}{S_2} = \frac{\sqrt{K_p}}{\sigma_2 R_2} (P)^{-1/2} + \delta. \quad (6)$$

K_p is the equilibrium constant for thermal dissociation, P is the total pressure of $A + A_2$ in the source, and σ_2 and R_2 are the ionization cross section and detectivity of the molecule relative to the atom, respectively.

Thus, a plot of S_1/S_2 vs $(P)^{-1/2}$ should give a straight line with slope $(\sqrt{K_p}/\sigma_2 R_2)$ and intercept δ . K_p is defined by the gas temperature, and values for σ_2 are available in the literature²⁸; hence, R_2 can be determined from these plots as well as δ . Some sample plots of S_1/S_2 vs $(P)^{-1/2}$ are given in Fig. 4.

Once δ had been determined, the relative atomic densities under different beam conditions were calculated using Eq. (5). These densities were monitored

TABLE I. Relative H and D densities in the seeded beams.

Seeding gas	Fraction H ₂ (D ₂)	Total pressure (psig)	I_{rel}^a	$[H]_{\text{rel}}^b$
(a) H atom beams				
H ₂	100%	10	[1.00]	[1.00]
He	20%	12	0.19	0.27
Ne	18%	14	0.05	0.14
(b) D atom beams				
D ₂	100%	10	0.71	1.00
Ne	17%	15	0.062	0.19
Ar	18%	20	0.032	0.13

^aH(D) atom intensity relative to the intensity of a 10 psig H₂ beam $\sim 10^{16}$ atoms cm⁻² s⁻¹ 10 cm from the nozzle.

^bH(D) atom density relative to the density of a 10 psig H₂ beam ($\sim 4 \times 10^{-7}$ Torr) 10 cm from the nozzle.

during every run. Some sample results are given in Table I.

These data showed a dramatic decrease in atomic intensity as the mass of the seeding gas was increased. This is a well known effect in seeded beams, in which the lighter gas species is scattered out of the beam during the expansion. This created some experimental difficulty when the very slow H and D atomic beams were used, as the fraction of hydrogen in the gas mixture could not be increased any more without sacrificing the low velocity.

In order to measure the velocity distributions of the beam constituents, time-of-flight (TOF) spectroscopy was used. To do this, the beam modulation chopper was removed and a high speed chopper installed on the skimmer mounting plate. The resulting flight path was 100 cm, which allowed accurate determination of particle velocities.

One of the problems was the determination of the gas temperature for a given source temperature, as the two were not necessarily the same. Lee and co-workers²⁹ observed that for their oven the gas temperature (measured by TOF of inert gases) was 20% lower than the measured source temperature at 2000 K. This was caused by the extreme thermal gradient (their source was 2000 K at the orifice, and water cooled at the end) and the large flow velocity through the source. The oven used for the present experiments also had a temperature gradient and an even larger flow velocity, so the same effect could be expected. From TOF spectra of He, Ne, and Ar at various temperatures it was found that the gas temperature of the beam was lower than the source temperature (measured by optical pyrometry). The results of these experiments are given in Fig. 5, where the temperature determined by the TOF spectra for He, Ne, and Ar beams has been plotted against the temperature reading of the optical pyrometer. The solid line is the oven temperature, and the dotted line is the gas temperature.

Finally, we measured the TOF spectra of the beam

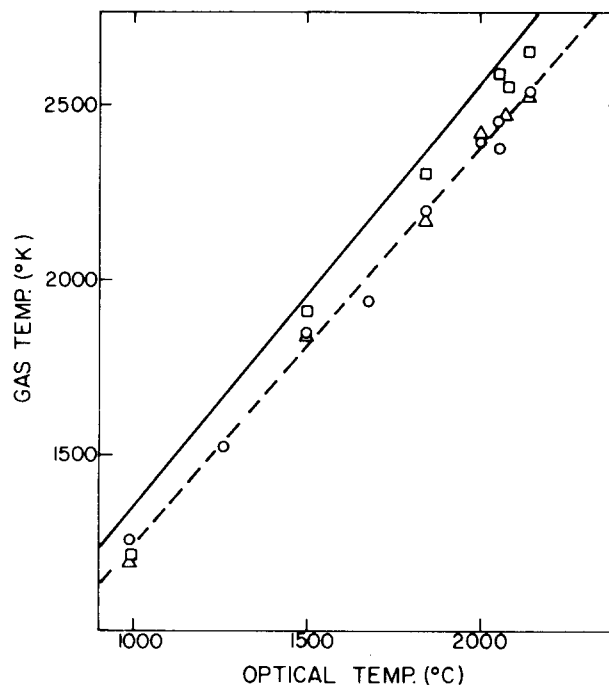


FIG. 5. Gas temperature measured by TOF plotted against the reading of the optical pyrometer. The abscissa is in °C since the optical pyrometer is calibrated in these units. The solid line gives the actual temperature of a W oven for a given pyrometer reading. The data points are the gas temperature determined from the TOF spectra of He (triangles), Ne (circles), and Ar (squares) supersonic beams. The dotted line gives gas temperature for a given optical pyrometer reading.

constituents under a variety of seeding conditions. The most probable velocities and Mach numbers for typical operating conditions are given in Table II. In Fig. 6 the peak velocities for the beam constituents have been plotted as a function of the fraction of H₂ in the mixture, for H₂/He and H₂/Ne beams. The solid lines show what would be expected for mixtures of ideal gases.

The data showed that the velocity trend was correctly predicted by the ideal gas equations, but that there was slippage, i.e., the H atoms had a higher velocity than the diluent gas used to slow down the H. This would be expected.²⁹ The amount of slippage is not excessive in view of the relatively high concentrations of H₂ and D₂ used in these mixtures.

The energy distributions for typical atomic H and D beams are given in Fig. 7. The distributions shown are calculated from the parameters listed in Table II.

F. HBr and DBr: Sources and reagents

To produce a partially collimated effusive beam of molecular reagents, multicapillary array sources were used. The sources used in these experiments were 13 mm diameter glass multicapillary arrays with 50% open area, consisting of 25 μ diameter holes. These arrays were epoxied onto the ends of 1 cm bore Pyrex tubing. Separate sources were used for HBr and DBr and these were positioned on top of one another about 3 cm from the center of the PMT, at 90° to the atomic beam. (In earlier experiments we found that when

TABLE II. Beam velocities and Mach number for H and D beams.

Gas mixture	Total pressure (psig)	H(D)		H ₂ (D ₂)		Inert gas	
		v_{mp} ^a	M_T	v_{mp}	M_T	v_{mp}	M_T
Pure H ₂	10	7.69	7.	7.69	7.
12% H ₂ in He	15	5.32	5.	5.38	5.	5.18	6.
27% H ₂ in Ne	22	2.7	... ^b	2.72	5.	2.48	8.
Pure D ₂	10	5.40	8.	5.40	8.
16% D ₂ in Ne	17	3.13	5.	3.13	6.	2.91	8.
15% D ₂ in Ar	15	2.2	... ^b	2.15	5.	2.05	8.

^aVelocity in km/s.^bInadequate signal to measure accurately.

using the same source, but with 5 μ holes, the increased divergence of the beam led to attenuation of the primary beam before the viewing region, as well as clogging of the arrays.)

To maintain a steady flow, the DBr or HBr was kept in a dry ice/acetone bath, which provided around 400 Torr vapor pressure. At high flows, the baths were lowered to the top of the liquid HBr (thereby reducing the rate of cooling) to maintain the 400 Torr. The flows were controlled by a Monel fine metering valve and were measured by Fischer-Porter triflat flowmeters. The pressure in the array source was measured by a Hewlett-Packard quartz spiral gauge.

The HBr used in these experiments was obtained from Matheson (99.8% purity). It was taken from the cylinder through a Monel needle valve and frozen in the HBr storage trap (cooled by liquid nitrogen) until there was sufficient HBr trapped. The HBr was then degassed by a few freeze-thaw cycles and was stored in a dry ice/acetone bath for use.

The DBr was synthesized by the method of Wilson and Wylie.³⁰ Once made, the DBr was used in the same manner as the HBr. The purity of the DBr was checked by measuring the infrared absorption spectrum of 400 Torr of DBr in a 10 cm path cell. In all experiments the DBr was of > 95% isotopic purity.

The hydrogen used in these experiments was UHP grade, obtained from Matheson (99.999% pure). The deuterium was C. P. grade from Matheson (99.5% isotopic purity). All inert diluent gases used in the supersonic source were obtained from Matheson. He and Ar were UHP grade (99.999%) and Ne was "purified" (99.99%). All gases were used without further purification.

G. Experimental procedure

To align the apparatus for the crossed molecular beam experiments, the VUV probe laser path through the main chamber and the supersonic atomic beam axis

were defined by two He-Ne laser beams. The reaction zone was at the crossing point of these two lasers. All the components of the apparatus were aligned with respect to these He-Ne laser beams. Once the apparatus was aligned, it was evacuated to the operating pressure, and the experiment was performed.

Before collecting data, the mass spectrometer was checked by monitoring a 300 K H₂ beam. At the same time, the VUV laser was aligned as described above.

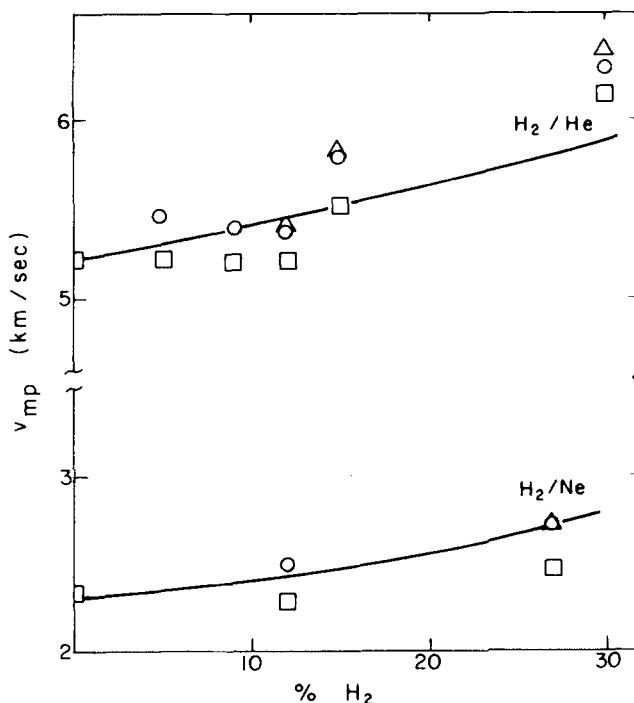


FIG. 6. Results of TOF velocity analysis of seeded atomic H beams. The most probable velocity measured is plotted as a function of the percentage of H₂ in the source gas mixture. The data points are as follows: triangles—H atoms; circles—H molecules; squares—noble gas. The continuous curves are the v_{mp} expected for an ideal mixture of the stated composition.

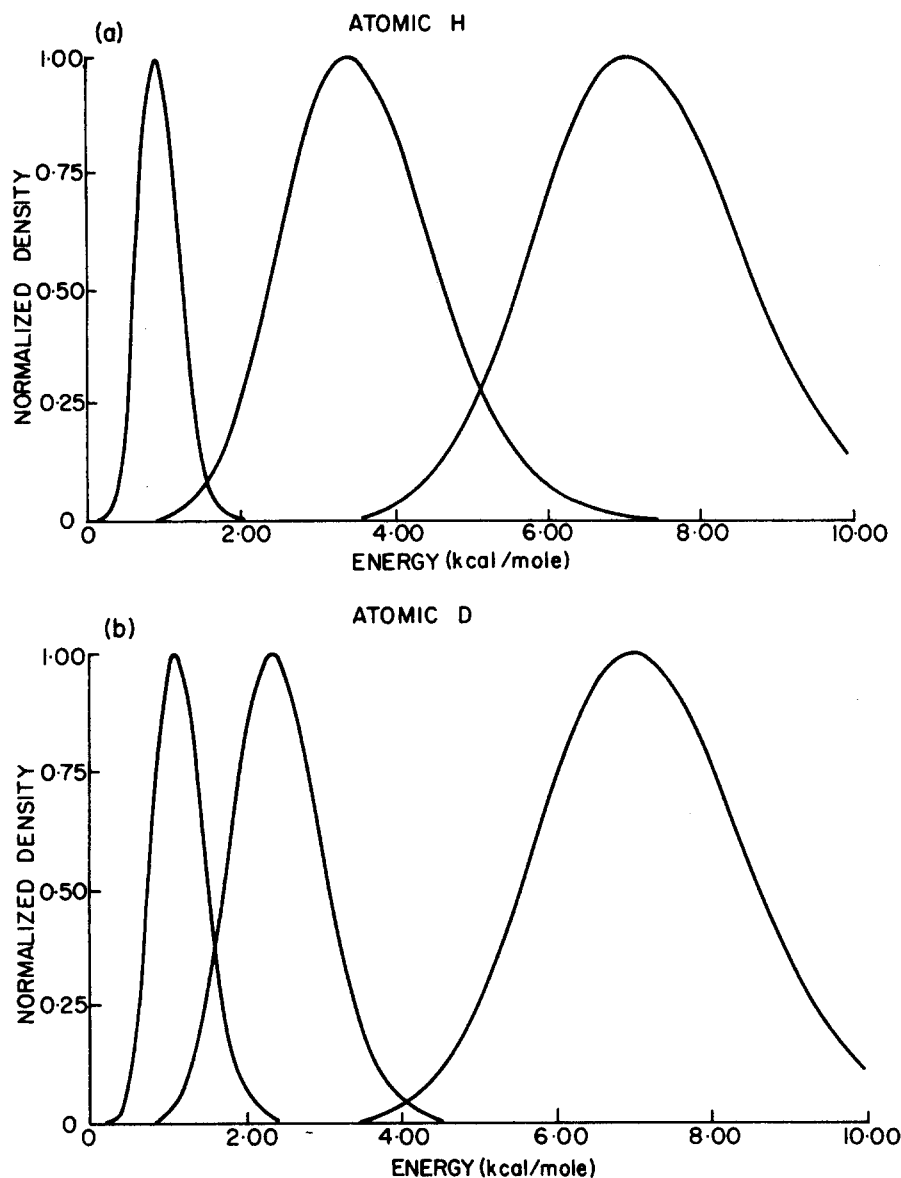


FIG. 7. Energy distributions for H and D atom supersonic beams. The velocity distributions used for these plots were determined by TOF spectroscopy; their parameters are given in Table I. The oven temperature was 2700 K in all cases.

If both of these systems were working, the hydrogen oven was brought to operating temperature and aligned (using external adjustment screws) by maximizing the beam signal seen by the mass spectrometer.

Throughout the experiment, a reference VUV fluorescence signal was measured periodically. This was done by using standard reagent flow conditions which could be reproduced easily. This standard was 10 psig of H_2 in the supersonic source oven, with a flow of 25–30 $\mu\text{mol/s}$ of HBr. The initial ν_2 tuning was obtained by maximizing the 1541 Å resonance fluorescence signal from the reaction under standard flow conditions.

After the reference had been established, data were collected at several HBr and DBr flows for a given H atom source gas mixture. Data collection was interrupted frequently so that the H or D atom density could be monitored in the absence of molecular flow. Between different gas mixtures for the H (or D) source, a measurement of the reference fluorescence signal

was taken. This reference showed a variation in signal detectivity only during experiments on the H (D) + Br_2 reaction.⁴ In this case the detectivity varied linearly with time so a correction could be made. In all the experiments reported here, no variation outside the experimental uncertainty was ever seen.

The DBr source was deuterated by flowing DBr through it for 10 or 15 min before data collection. In order to compare data taken with different sources, fluorescence signals were measured under several flow conditions with HBr coming from the DBr source and *vice versa*. It was typically found that signals with the DBr source were about 30% higher than those with the HBr source.

In all experiments a check was made for scattered light and other interfering signals by tuning ν_2 off resonance. Resonance signals were also looked for with either the HBr (DBr) or atomic beam off. No signal was seen under any of these conditions in any of the experiments.

III. RESULTS AND DATA ANALYSIS

Under proper conditions, the fluorescence signal measured in a LIF experiment is proportional to the density of the detected species.^{2,31} Thus, for these experiments

$$[\text{Br}] \propto I_{\text{SIG}}/I_{\text{VUV}} \quad (7)$$

$[\text{Br}]$ is the atomic Br product density in the viewing zone, and I_{SIG} and I_{VUV} are the fluorescence signal and the VUV laser intensity, respectively. In order to check the validity of Eq. (7), a small density of Br atoms was formed in the reaction zone, either by CO_2 laser multiphoton dissociation of CF_3Br or by reaction of $\text{H} + \text{HBr}$, and I_{SIG} was measured as a function of I_{VUV} . Several such experiments were performed. In all cases, plots of I_{SIG} as a function of I_{VUV} were linear, and had a zero intercept.

The VUV laser linewidth was determined to be $0.8\text{--}1.0 \text{ cm}^{-1}$ by looking at the (0,0) band of the fourth positive system of the CO spectrum at about 1540 \AA . This linewidth is approximately a factor of 2 larger than the total Br resonance-line linewidth (Doppler width plus hyperfine splitting); consequently, it was not necessary to make line shape corrections in Eq. (7).

The steady-state density of Br atoms in the viewing zone is the result of the competition of reactive formation of Br in the viewing zone and diffusion out. This means that in order to obtain cross sections from the measured $[\text{Br}]$, a correction must be made for the rate of diffusion, which is proportional to v_{Br} , the lab frame velocity of the Br atomic product.³¹ As we are dealing with a well-defined reagent relative velocity v_{rel} , we directly measure the total reactive cross sections in these experiments; the major uncertainties stem from the present state of knowledge regarding the product velocity distribution from this reaction. The expression for the reactive cross section is

$$S_r \propto I_{\text{SIG}} \cdot v_{\text{Br}} \cdot (I_{\text{VUV}} \cdot [\text{H}] [\text{HBr}] \cdot v_{\text{rel}}^{-1}) \quad (8)$$

In the experiments performed, I_{SIG} , I_{VUV} , $[\text{H}]$, and v_{rel} were measured directly, as discussed in the Experimental section. In order to check that the density of atomic reagent monitored by the mass spectrometer was the same as the density in the reaction zone, we performed several control experiments described below. What was measured with the mass spectrometer was the atomic density on the central axis of the supersonic beam. The mass spectrometer sampled the central 0.2° of the beam, while the actual beam was only collimated to a 3.5° half-width. We have made checks which would show any errors due to variation in atomic density across the beam, with alteration in the seeding gas although we do not expect errors due to this cause in view of the small angles involved.

In the first check for a given HBr (DBr) flow and seeding gas, data were recorded for two different seeding-gas mixtures. This meant that the only thing that changed was the H(D) atomic density in the reaction zone. This density was measured by mass spectrometry as described previously and the data obtained were used in Eq. (8) to calculate the cross section for

the two gas mixtures. In seven such pairs of determinations, the values of S_r were the same to within experimental error.

A second check was provided in a previous experiment,⁴ where the cross section for the reaction $\text{D} + \text{Br}_2 \rightarrow \text{DBr} + \text{Br}$ was determined at $E_T = 7 \text{ kcal/mole}$ using two different supersonic D beams. One beam used pure D_2 in the oven, and the other a D_2/He gas mixture. Once again the measured cross sections were the same.

To determine the density of molecular reagent in the reaction volume, the flow of reagent was measured, and a relationship was obtained between flow and density.

For a multicapillary array source, it is known that the divergence of the beam increases as the driving pressure increases.³² The beam from this source is quite well collimated at low flows, and the viewing zone is fairly large ($\sim 2\text{--}3 \text{ cm}$ in diameter), so it is the average density of reagent over the viewing zone we are concerned with in Eq. (8), and not the center-line density. This would be expected to behave as²⁹

$$[\text{HBr}] \propto [\text{flow}(\text{HBr})]^y, \quad (9)$$

where y is between 0.5 and 1.0.

If $\log(I_{\text{SIG}}/I_{\text{VUV}})$ is plotted as a function of $\log[\text{flow}(\text{HBr})]$, the slope is y in Eq. (9). Some results are given in Fig. 8. The slope of the plots was 0.7 regardless of the atomic beam used. The average of 20 such plots was 0.70 ± 0.08 . In order to provide a further check on the density relation given in Eq. (9) the attenuation of the atomic beam was examined as a function of flow. The attenuation of a beam should depend on the density of scattering gas in a Beer's law fashion.³³ We observed this behavior in several experiments, when $(\text{flow})^{0.7}$ was used as a measure of the HBr or DBr density.

In the course of an experiment, all of the parameters of Eq. (8) were measured directly (as described above) except for the lab velocity of the Br atom product v_{Br} .

One possible source of error in Eq. (8) stems from the use of a single velocity v_{Br} . We checked this by doing a complete integration over sample three dimensional differential cross sections for this reaction (and others⁴) and comparing this with the result of simply multiplying by the most probable velocity v_{Br} . In all cases studied there was less than 5% difference in the cross section resulting from the two approaches.

The real problem in performing the density-to-flux transformation embodied in v_{Br} lies in the lack of information at the present time concerning the differential cross section for this reaction, so an approximate differential cross section had to be obtained from dynamical considerations, as described below.

In the HHX system, a collinear activated complex is expected due to the interaction of the two 1s H atoms.³⁴ This is seen with LEPS potential energy surfaces for these systems.³⁵ *Ab initio* results also confirm this preference for a collinear geometry.³⁶ The reaction

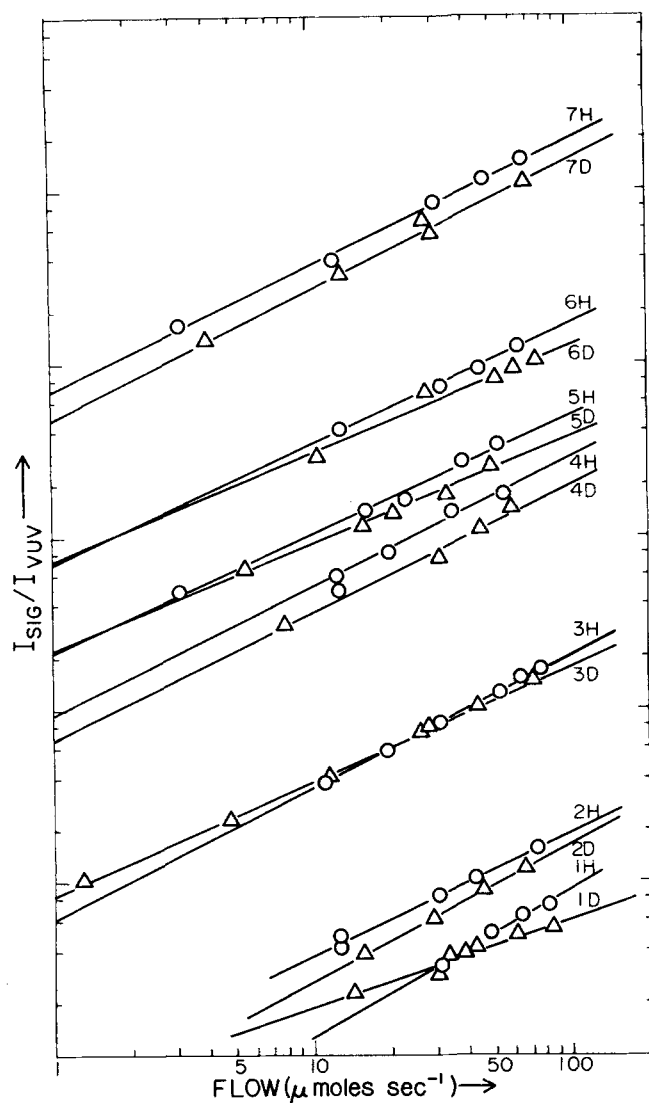


FIG. 8. The logarithm of $I_{\text{SIG}}/I_{\text{VUV}}$ is plotted against the logarithm of the HBr or DBr flow. The numbers indicate data measured with the same atomic source gas mixture, with the H standing for HBr, and the D for DBr. Data points for HBr are circles, and for DBr are triangles. The data sets are as follows: (1) H, D— D_2 in Ar + HBr, DBr; (2) H, D— D_2 in Ne + HBr, DBr; (3) H, D—Pure D_2 + HBr, DBr; (4) H, D— H_2 in Ne (mixture II) + HBr, DBr; (5) H, D— H_2 in He + HBr, DBr; (6) H, D— H_2 in Ne (mixture I) + HBr, DBr; (7) H, D—Pure H_2 + HBr, DBr.

studied in these experiments is known to have a relatively small cross section.^{6,7} This, combined with the collinear geometry, would be expected to cause the products to rebound back along their lines of approach, as viewed in the center of mass. This expectation gains credence from the observation that the mass combination $L + LH$ gives backward scattering in all but the most "attractive" energy surfaces.³⁷ The small cross section would lead one to expect something other than a highly attractive energy surface (long range attraction is associated with large cross sections). In fact, this expectation of rebound reaction was confirmed in a trajectory study by White,³⁸ which showed the molecular product of the $\text{H}' + \text{H}''\text{Br}$ reaction to be sharply backward scattered.

Accordingly, the data reported here were analyzed assuming that the $\text{H}'\text{H}''$ was backward scattered in the center of mass, and hence Br was forward scattered.

In order to calculate v_{Br} , knowledge of the product energy distribution was also required. Again, no experimental data are available for this reaction. White's trajectory studies showed 60% of the available energy going into internal excitation in the H_2 .³⁸ Typically, internal excitation accounts for 50%–70% of the energy release in the three-atom exchange reactions that have been studied experimentally³⁹; this appears to be a plausible figure. White's results indicated that 40% of the available energy went into product translation. Reagent translational energy in excess of the energy barrier (> 1 kcal/mol) was assumed to be efficiently ($\sim 80\%$) transformed into product translation, as has been found to be the case in several experimental and theoretical studies.⁴⁰

To sum up, the product velocities given in Table III were calculated assuming that 40% of the exothermicity plus 80% of E_T went into translational energy in the products.

Fortunately, the relative values of v_{Br} with variation in E_T that determine the measured quantity, which is S_r as a function of E_T , are not very sensitive to the product energy distribution assumed. If, for example, one assumes that all of the available energy (exothermicity plus E_T) goes into product translation, or alternatively that a fixed 40% of the available energy goes into translation, the change in v_{Br} over the range of E_T used here is only altered by 5%.

Moreover, results are not affected by moderate changes in the differential cross section. If one assumes that the H_2 product peaks at 150° in the center of mass, rather than 180° , the values of v_{Br} show change by no more than 2%.

The Newton diagrams for the two extreme values of E_T used in these experiments are given in Fig. 9.

The cross sections obtained from the experimental data using Eq. (8) are given in Fig. 10. All S_r are normalized with respect to the cross section of $\text{H} + \text{HBr}$

TABLE III. Br atom laboratory frame velocities.^a

Seeding gas	E_T^b	Molecular reagent	
		HBr	DBr
(a) H atom beams			
H_2	7.00	0.382(1.00)	0.407(1.05)
He	5.41	0.355(0.93)	0.380(0.99)
Ne	0.89	0.310(0.81)	0.334(0.87)
(b) D atom beams			
D_2	6.82	0.44(1.15)	0.46(1.20)
Ne	2.29	0.365(0.96)	0.38(1.00)
Ar	1.25	0.335(0.88)	0.352(0.92)

^aVelocities are given in km/s with the velocity relative to (H, H) at $E_T = 7$ kcal/mol in brackets.

^bIn kcal/mol.

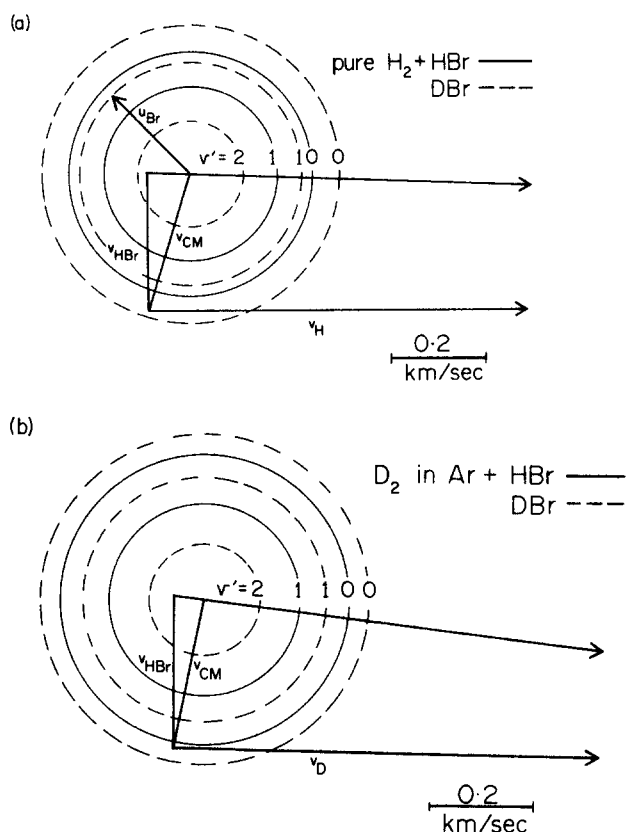


FIG. 9. Newton diagrams: (a) H+Br (DBr) at $E_T=7.0$ kcal/mol; (b) D+HBr (DBr) at $E_T=1.23$ kcal/mol. Velocities of Br atoms in the center of mass are shown as circles, labeled according to the product vibrational state (v').

at $E_T=7$ kcal/mol (set equal to unity). The data are the result of five separate experiments performed on different days. For each experiment S_r , for a given collision energy and reaction, is the average of several values measured under different flow conditions. After the values of S_r for any particular experiment were normalized, the data for all five experiments were averaged. The error limits shown represent one standard deviation in the normalized cross sections, and thus include the uncertainty of S_r for H+HBr at $E_T=7$ kcal/mol. In any given experiment, the variance in the values of S_r for H+HBr at $E_T=7$ kcal/mol was 5%–10%.

IV. DISCUSSION

A. Excitation functions

As can be seen in Fig. 10, no threshold for reaction was observed over the energy range studied in these experiments (0.97–7.0 kcal/mol). The threshold energy for the abstraction reaction must therefore lie below 0.9 kcal/mol. If we describe the D+HBr (DBr) data by a line-of-centers energy dependence³³

$$S_r = S_0 (1 - E_0/E_T), \quad (10)$$

we obtain a threshold energy $E_0 = 0.16$ kcal/mol.

The excitation functions appear to be significantly

different for H and D atomic reagents. The cross section for the reaction of H atoms declines slightly over the range of E_T investigated, while S_r for D atoms increases slightly. However, in view of the fact that the changes in S_r are comparable to the experimental uncertainties, and in view of the uncertainty involved in the flux correction (the v_{Br} term) due to the lack of detailed knowledge concerning the reaction dynamics, our experiments in isolation do not clearly demonstrate a difference between the excitation functions for H and D atoms. We shall discuss these differences further in the final section, where previous thermal studies will be considered.

Two classical trajectory studies (performed prior to the present experiments) assist in bridging the gap between the observed excitation functions and the HHBr potential. In both of these studies the excitation function [$S_r(E_T)$] was calculated for the H+DBr reaction, and in both the LEPS semiempirical potential energy surface was employed. The results are summarized in Fig. 11, together with the present data for the H+DBr reaction.

The first study, by Parr and Kupperman³⁵ (P-K), used a surface which had a 1.75 kcal/mol barrier to abstraction, and a 3.95 kcal/mol barrier to exchange.

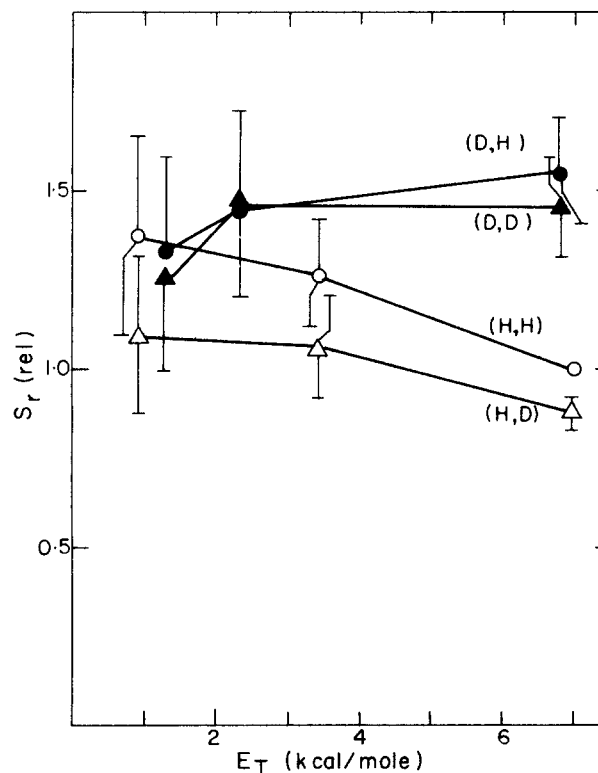


FIG. 10. Relative cross sections for the reaction $H'+H''Br \rightarrow H'H''+Br$ are plotted as a function of the collision energy E_T . Labeling of the cross sections is according to the (H' , H'') convention used in the text, with circles being used for the HBr data and triangles for the DBr data. Filled symbols indicate D atom data and open symbols the H atom data. All S_r are relative to the cross section for (H,H) at $E_T=7$ kcal/mol. Lines connect data points for the same isotopic combinations. Error bars are defined in the text.

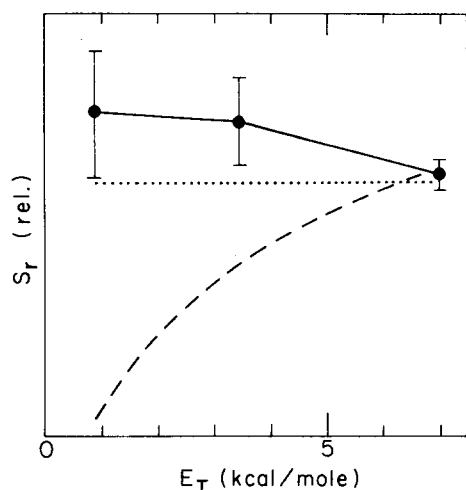


FIG. 11. Results of trajectory studies on H+DBr. Experimental results from the present study are given as the filled circles. Trajectory results from Parr and Kupperman (dashed line) and White (dotted line) are plotted on the same scale; the S_r calculated by trajectories are normalized to the $E_T=7.0$ kcal/mol experimental point.

The P-K surface had no attractive hollows. It can be seen in Fig. 11 that even the 1.75 kcal/mol barrier to abstraction exceeds the actual value, since the computed $S_r(E_T)$ shows a definite threshold behavior not seen in the experiments.

The second study, by White and co-workers,^{38,41} employed a modified LEPS surface with no barrier to abstraction and 1 kcal/mol barrier to exchange. This surface (the W surface) did have three potential wells of significant depth (2–3 kcal/mol). Trajectories run on the W surface do reproduce the measured $S_r(E_T)$ quite well, supporting the contention (above) that the barrier to abstraction is negligible.

While the agreement of White's trajectory results with our measured cross sections is encouraging, the W surface gives too much exchange reaction at low energies, since the barrier in the HBrH configuration is too small. The barrier to exchange should be on the order of 5 kcal/mol or greater.^{6,42} The second fault with the W surface is the presence of deep wells, which elastic scattering experiments by Toennies and co-workers⁴³ have shown not to exist in this system.

In summary, it would appear that the potential-energy surface for the H+HBr system has the following properties: a negligible barrier (<1 kcal/mol) in the HHBr configuration,⁴ a barrier of about 5 kcal/mol in the HBrH configuration,⁶ and no attractive wells in either configuration.⁴³

B. High energy isotope effects

In this study, the effect of isotopic substitution on reaction cross section was measured at several different (nonoverlapping) collision energies. At 7 kcal/mol collision energy the order of reactivity found was (D, H)>(D, D)>(H, H)>(H, D). As the collision energy decreased, the isotope effect seemed to change,

and at $E_T=1$ kcal/mol the ordering may be different. Because of the large error limits at $E_T=1$ kcal/mol, we cannot make a definite statement about this change based only on our data. We shall return to this point in the following section, in which the present data will be discussed in combination with thermal studies performed on these reactions.

At high collision energies, one would expect any effects due to an energy threshold to be insignificant, so that kinematic effects dominate. Our high energy reactive cross sections have the least uncertainty, due to maximal H or D atom reagent flux. In what follows we discuss the order of reactivity observed for $E_T=7$ kcal/mol in terms of simple kinematics.

In Table IV the scaling and skewing parameters for Reactions (1) through (4) are given. These take account only of collinear kinematic effects. The ordering implied by the skewing and scaling parameters appears to be in conflict with the experimental findings. It is plausible that increased skewing correlates with decreased reactivity¹⁶ and increased scaling parameter β —indicative of a narrow exit valley leading out of a broader entry valley—results in decreased reactivity.³⁷ However, for (H, H) and (D, H), neglecting the small changes in scaling, the ordering based on skew angles is (H, D)>(D, H), directly contrary to what is observed (Fig. 10).

The conjectures regarding the ordering based on skewing and scaling of the collinear potential energy surface were substantiated by a trajectory study performed in this laboratory⁴⁴ using the P-K surface. The results of a batch of collinear trajectories showed a sequence of cross sections (D, D)>(H, D)>(H, H)>(D, H). This clearly does not agree with experiment. It would appear that the small changes in skewing and scaling, i.e., the collinear kinematic effects, cannot account for the observed isotope effect.

However, when trajectories were run on the same surface in three dimensions, qualitative agreement with experiment was obtained. The overall ordering seen [(D, H)>(H, H)>(D, D)>(H, D)] was in fair accord with that observed, except for the reversal of (H, D) and (D, D). The success of a three dimensional trajectory study where a collinear study on the same surface failed suggests that rotation plays an important part in accounting for the effect of changing masses.^{14–16}

The cause of these rotational effects is the preferred collinear geometry of the reactive intermediate in HHX systems. This geometry can be understood in terms of

TABLE IV. Scaling and skewing in H'H''Br.

System	Skew angle ^a	Scaling parameter β^a
H H Br	45.6°	0.712
H D Br	55.2°	0.584
D H Br	35.8°	0.822
D D Br	45.7°	0.716

^aAs defined in Ref. 46; (approach coordinate)/(retreat coordinate).

simple valence bond arguments³⁴ as both the attacking atom and the atom under attack are 1s in character. *Ab initio* calculations also give the collinear geometry as having the lowest energy in HHX.³⁶

The LEPS semiempirical potential energy surface, which describes these reactive systems successfully, has a well known bias favoring collinear approach of reagents.³⁴ For the HBr system, the LEPS surface predicts a very narrow cone of approach for an H atom attacking at the H end of HBr (the P-K surface has a 34° cone of approach at 3.5 kcal/mol collision energy). To be reactive, the attacking H atom must approach the HBr within this cone; a rotational alignment of the HBr toward a more collinear geometry, during the course of collision, will effectively widen this cone of approach, increasing the probability of reaction.

The cause of this rotational alignment is the torque exerted on the HBr molecule as the H atom approaches. The source of the torque is the lowering in potential energy as the reaction complex approaches collinearity. Adding to the torque caused by this relative stability is a potential well which appears in the collinear configuration when the bond under attack is stretched due to vibration.⁴⁴

Similar alignment effects have been noted in earlier theoretical studies.¹⁴⁻¹⁶ A model study on mass effects in exchange reactions¹⁴ showed the differing effect on reactive cross section of alignment forces for two contrasting mass combinations $L + HH$ (light+heavy-heavy) and $H + LH$ (heavy+light-heavy); the alignment effect was observed on markedly differing energy surfaces. Later studies on $H + H_2$ ¹⁵ and its isotopic variants¹⁵ also showed some alignment. In all cases, the favorable circumstance was a heavy attacking atom (lengthened interaction time) and a low moment of inertia for the molecule under attack (decreased rotational period). This agrees with the experimental observation in the present work that the cross section for $(D, H) > (H, D)$ at enhanced collision energy, for which kinematic effects should dominate.

Since these effects have been documented in 3D trajectory studies, it is instructive to examine them in terms of a simple model for reaction. We shall suppose that for abstraction to occur the attacking H' atom must approach the H''Br by a nearly collinear path at the H'' end. If we assume that the reactive cross section is proportional to the magnitude of the "cone of acceptance" at the H'' end of H''Br,³⁵ then we need only calculate the *effective* cone of acceptance of H''Br—taking into account alignment of H'H''Br—to get the relative cross sections for various (H', H'').

To simplify the problem further, we assume that the aligning force is applied for a small period of time τ , while the system is in a critical configuration. This is similar in spirit to models of chemical reactions in which the reaction exothermicity is released during a brief period while the nascent products separate.^{37,45} A further assumption that will be made is that only those complexes that can be aligned into a collinear

configuration in the time τ will react. Thus, the cone of acceptance will be defined by the maximum bending angle ϕ_{\max} of the H'H''Br complex that can be brought into alignment during interaction time τ under the influence of the force constant characteristic of the activated state.

To describe the alignment process, we shall use a harmonic oscillator model for the bent H'H''Br. If A is the amplitude of the bending vibration of the complex and the initial approach angle is ϕ , then the angle that the H'H''Br is bent away from collinearity at a time t is given by (Fig. 12).

$$\theta(t) = A \cos(\omega_{\theta} t - \delta) \quad (11)$$

where δ is the initial phase of the bending vibration, related to the approach angle ϕ as $\delta = \cos^{-1}(\phi/A)$. The "aligning force" is contained in the frequency of the bending vibration ω_{θ} . We use the BEBO method⁴⁶ to obtain the activated configuration, and also ω_{θ} . For HBr, the barrier is at $r_{\text{HH}}^{\ddagger} = 1.45 \text{ \AA}$ and the bending frequency is $\omega_{\theta} = 343 \text{ cm}^{-1}$.

The choice of the barrier as the location of the alignment is based on the knowledge that for $H + HBr$, and most other $A + BC$ systems, there is little long range attraction between the A and the BC. Thus, the alignment force is likely to be the result of short range repulsive interaction at the barrier crest. For the $H + HBr$ system a potential fitted to recent scattering results⁴³ allows H' to approach to $r_{\text{H'H''}} = 1.8 \text{ \AA}$ at a collision energy of 7 kcal/mol.

We can use this same potential to determine the interaction time τ to be used in Eq. (11) by determining how long it takes an attacking H' atom to reach the turning point, starting from the position to zero potential energy between H' and H''Br. The position of zero interaction is at $r_{\text{HH}} = 2.5 \text{ \AA}$. With an initial velocity of 8 km/s ($E_T = 7 \text{ kcal/mol}$) it takes the H' atom $1.1 \times 10^{-14} \text{ s}$ to get to $r_{\text{HH}} = 1.8 \text{ \AA}$ (D atoms will take $1.6 \times 10^{-14} \text{ s}$). These were the interaction times used in the present model calculation.

The cone of acceptance is given by the maximum angle of approach ϕ_{\max} that will give $\theta(\tau) = 0^\circ$ when used in

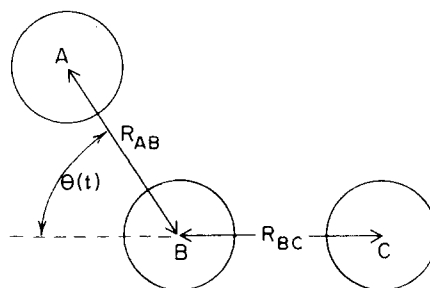


FIG. 12. Alignment model for $A + BC$ reactions. The ABC complex is shown in a critical configuration, from which alignment occurs. In this case, $A = H'$, $BC = H''Br$. $\theta(t)$ at $t = 0$, i.e., the initial approach angle, is defined as ϕ . The maximum ϕ from which alignment can occur in a time τ is ϕ_{\max} [i.e., for ϕ_{\max} , $\theta(\tau) = 0^\circ$].

Eq. (11). The relative cross sections are then given by the solid angle subtended by the cone of acceptance, i. e., $S_r \propto 1 - \cos \phi_{\max}$. The results of these calculations are given in Table V.

While it is gratifying that the model correctly predicts the magnitude of the (D, H) to (H, D) isotope effect, it is more important to note that the ordering for these two extreme cases is correct. Based on the model, (D, D) and (H, H) should be equally reactive—some effect other than alignment may account for (D, D) being more reactive than (H, H).

C. Comparison with thermal data

In this section previous thermal studies on the abstraction reactions (1) to (4) will be examined in light of the data at controlled collision energies taken from the present experiments. The thermal data can provide information on the behavior of the HHBr system averaged over low collision energies. The measured temperature dependence of the reaction rates for Reactions (1) through (4) will be examined first. When these data are combined with the present data on the dependence of S_r on E_T , information can be obtained on the dependence of S_r on the internal energy of DBr or HBr.

There has been little direct measurement of reaction rates in the H + HBr system reported in the literature.^{6,7,47} In only one case was the thermal reaction rate for the abstraction reactions measured as a function of temperature; in this study Endo and Glass⁶ found that the reaction rates for the abstraction reactions increased by about fourfold over the temperature range 230 to 318 K. This led to activation energies which ranged from 1.69 to 2.57 kcal/mol. They concluded from these results that the barrier height on the HHBr surface must be ~ 2 kcal/mol. Our results definitely indicate a smaller translational energy barrier than this, as has already been discussed. We have directly measured the excitation function for the abstraction reactions down to low energies. It is well known^{37,48} that the rate constant for a reaction can be obtained by convoluting the excitation function with the Maxwell-Boltzmann distribution

$$k(T) = (\pi\mu)^{-1/2} (2/kT)^{3/2} \int_0^\infty S_r(E) E \exp(-E/kT) dE. \quad (12)$$

The result of Eq. (12) is based on the assumption that $S_r(E)$ depends only on the collision energy. However, when the reagent temperature is varied, the in-

TABLE V. Results of the alignment model calculation.

Reaction	ω_θ^a	τ^b	ϕ_{\max}	S_r (calc.) ^c	S_r (expt.) ^d
(H, H)	6.44	1.1	27°	[1.00]	[1.00]
(H, D)	4.99	1.1	21°	0.64	0.89 ± 0.06
(D, H)	6.11	1.6	34°	1.58	1.56 ± 0.14
(D, D)	4.56	1.6	27°	1.00	1.46 ± 0.14

^aIn units of 10^{13} rad/s.

^bIn units of 10^{-14} s.

^cNormalized to (H, H).

^dRelative S_r for $E_T = 7.0$ kcal/mol.

TABLE VI. Rate constants and isotope effects for H' + H'' Br at 300 K.

Reaction	Endo and Glass ^a	Husain and Slater ^b
(a) Rate constants (10^{-12} cm ³ molecule ⁻¹ s ⁻¹)		
(H, H)	3.71 ± 0.14	6.0 ± 0.1
(H, D)	2.69 ± 0.13	4.7 ± 0.1
(D, H)	1.69 ± 0.13	4.1 ± 0.1
(D, D)	1.24 ± 0.15	2.7 ± 0.1
(b) Rate constant ratios		
(H, H)/(D, H)	2.20	1.46
(H, D)/(D, H)	1.59	1.15
(H, H)/(H, D)	1.38	1.28
(D, H)/(D, D)	1.36	1.52

^aReference 6.

^bReference 7.

ternal energy distribution also changes. In the specific example of H + HBr, the HBr becomes more rotationally excited (we neglect vibrational excitation since at these low temperatures all HBr is in $v = 0$). It is known that increased rotational energy can have a significant effect on the reactive cross sections.^{49,50}

We can test to see if rotational excitation affects the cross section by using our measured translational excitation functions in Eq. (12) to calculate rate constants at 230 and 318 K.

To describe the low energy behavior of $S_r(E)$, we have used three arbitrary forms to illustrate extremes possible in $k(T)$. The first of these $S_r(E) = \text{constant}$ will give a \sqrt{T} dependence for $k(T)$ and thus shows $k(T)$ increasing by 18% over the range 230 to 318 K.

At the opposite extreme in behavior of $S_r(E)$, we used a step function for $S_r(E)$, with the step at 0.8 kcal/mol. This functional form resulted in a 50% increase in $k(T)$ over the 230 to 318 K range.

The final form for $S_r(E)$ was given by Eq. (10) with $E_0 = 0.16$. This resulted in a 20% increase in $k(T)$ over the temperature interval.

All three functional forms were in accord with the measured $S_r(E_T)$ at low energy. Of the three excitation functions, the most plausible would be one resembling Eq. (10) in behavior.

The conclusion from these calculations is that the enhanced translational energy resulting from the increased temperature in Endo and Glass' work can only account for a change in $k(T)$ of less than 50%, rather than the observed increase by a factor of 4. It follows that for the abstraction reaction the average effect of increasing the rotational energy from 230 to 318 K is to increase the cross section of the reaction.

Next, we examine the rate constants at 300 K for all the isotopic variants of the abstraction reaction. Two studies on the H + HBr reaction^{6,7} show the same qualitative isotope effects, although the numerical values are different. The results of these studies are summarized in Table VI.

In order to compare the data obtained in the present beam experiments with the 300 K rate constants reported elsewhere,^{6,7} we have used several functional forms to describe $S_r(E_T)$. These functions passed through the median of the values for $S_r(E_T)$ given in Fig. 10. When the resulting $S_r(E_T)$ were introduced into Eq. (12), they yielded rate constant ratios that agreed to within 10% with $k(\text{H}, \text{D})/k(\text{D}, \text{H}) = 1.3$. This ratio lies between the two thermal measurements reported previously.^{6,7} Since the fitted $S_r(E_T)$ in all cases showed $S_r(\text{H}, \text{D}) < S_r(\text{D}, \text{H})$ at $E = 7 \text{ kcal mol}^{-1}$ and $S_r(\text{H}, \text{D}) > S_r(\text{D}, \text{H})$ as $E_T \rightarrow 0$, we believe that the 300 K thermal experiments taken together with our data (Fig. 10) imply a reversal in the isotopic sequence close to threshold.

It would seem from the foregoing that at lower collision energies the alignment of the H¹H²Br intermediate becomes less important in determining reactivity. This could be due to the fact that at larger τ (see the simple model described above) the system has time to align into the preferred collinear configuration whatever the isotopic composition.

ACKNOWLEDGMENTS

We are indebted to Professor M. Menzinger, Professor B. P. Stoicheff, and Professor S. C. Wallace for helpful discussions. J. W. H. and F. J. N. thank the Natural Sciences and Engineering Research Council of Canada (NSERC) for scholarships; J. C. P. is grateful to the Guggenheim Memorial Foundation for a Fellowship. This work was supported in part by NSERC, and in part by Atomic Energy of Canada Ltd.

- ¹H. W. Cruse, P. J. Dagdigian, and R. N. Zare, *Faraday Discuss. Chem. Soc.* **55**, 277 (1973); R. N. Zare and P. J. Dagdigian, *Science* **185**, 739 (1974); P. J. Dagdigian and R. N. Zare, *J. Chem. Phys.* **61**, 2464 (1974).
- ²J. L. Kinsey, *Annu. Rev. Phys. Chem.* **28**, 349 (1977).
- ³A. Gupta, D. S. Perry, and R. N. Zare, *J. Chem. Phys.* **72**, 6237 (1980), **72**, 6250 (1980).
- ⁴J. W. Hepburn, D. Klimek, K. Liu, J. C. Polanyi, and S. C. Wallace, *J. Chem. Phys.* **69**, 4311 (1978).
- ⁵An attempt was made to observe laser-induced fluorescence from $\text{Br}^* (^2P_{1/2})$ at 1532 Å. Under less than optimal conditions we obtained $S_r(\text{Br}^*)/S_r(\text{Br}) < 0.02$ (no fluorescence could be detected).
- ⁶H. Endo and G. P. Glass, *J. Phys. Chem.* **80**, 1519 (1976).
- ⁷D. Husain and N. K. H. Slater, *J. Chem. Soc. Faraday Trans. 2* **76**, 276 (1980).
- ⁸A. Persky and A. Kuppermann, *J. Chem. Phys.* **61**, 5035 (1974).
- ⁹H. Y. Su, J. M. White, L. M. Raff, and D. L. Thompson, *J. Chem. Phys.* **62**, 1435 (1975).
- ¹⁰J. D. MacDonald and D. R. Herschbach, *J. Chem. Phys.* **62**, 4740 (1975).
- ¹¹W. Bauer, L. Y. Rusin, and J. P. Toennies, *J. Chem. Phys.* **68**, 4490 (1978); W. H. Beck, R. Goetting, J. P. Toennies, and K. Winkelmann, *ibid.*, **72**, 2896 (1980); W. H. Beck, R. Goetting, J. P. Toennies, and K. Winkelmann, *Max-Planck-Institut für Strömungsforschung Bericht* **112/1979**.
- ¹²Haberland and co-workers have carried out extensive molecular beam studies on isotope effects in H and D atom reactions where the H or D atoms come from an effusive source. See H. Haberland, W. von Lucadou, and P. Rohwer, *Ber. Bunsenges. Phys. Chem.* **84**, 507 (1980), and references therein.
- ¹³S. Glasstone, K. J. Laidler, and H. Eyring, *The Theory of Rate Processes* (McGraw-Hill, New York, 1941); L. Melander, *Isotope Effects on Reaction Rates* (Ronald, New York, 1960).
- ¹⁴B. A. Hodgson and J. C. Polanyi, *J. Chem. Phys.* **55**, 4754 (1971).
- ¹⁵J. J. Wright, *J. Chem. Phys.* **69**, 720 (1978).
- ¹⁶H. R. Mayne, *J. Chem. Phys.* **73**, 217 (1980).
- ¹⁷N. Bloembergen, *Non-Linear Optics* (Benjamin, New York, 1965).
- ¹⁸J. J. Wynne, *J. Phys. (Paris), Colloq.* **39**, (1978).
- ¹⁹B. P. Stoicheff and S. C. Wallace, in *Tunable Lasers and Their Applications*, edited by A. Mooradian, T. Jaeger, and P. Stokseth (Springer, New York, 1976).
- ²⁰R. T. Hodgson, P. P. Sorokin, and J. J. Wynne, *Phys. Rev. Lett.* **32**, 343 (1974).
- ²¹S. C. Wallace and G. Zdasiuk, *Appl. Phys. Lett.* **28**, 449 (1976).
- ²²G. Zdasiuk, M.Sc. thesis, University of Toronto, 1975.
- ²³T. Hänsch, *Appl. Opt.* **11**, 895 (1972).
- ²⁴N. Aubauf, J. B. Anderson, R. P. Andres, J. B. Fenn, and D. G. H. Marsden, *Science* **155**, 977 (1967).
- ²⁵M. A. D. Fluendy, R. M. Martin, E. E. Muschlitz, and D. R. Herschbach, *J. Chem. Phys.* **46**, 2172 (1967).
- ²⁶F. E. Bartoszek, D. M. Manos, and J. C. Polanyi, *J. Chem. Phys.* **67**, 3396 (1977), and references therein.
- ²⁷J. W. Hepburn, Ph.D. thesis, University of Toronto, 1980.
- ²⁸L. J. Kieffer and G. H. Dunn, *Rev. Mod. Phys.* **38**, 1 (1966).
- ²⁹J. J. Valentini, M. J. Coggiola, and Y. T. Lee, *Rev. Sci. Instrum.* **48**, 58 (1977).
- ³⁰C. L. Wilson and A. W. Wylie, *J. Chem. Soc.* **1941**, 596.
- ³¹P. J. Dagdigian, H. W. Cruse, A. Schultz, and R. N. Zare, *J. Chem. Phys.* **61**, 4450 (1974).
- ³²J. C. Johnson, A. T. Stair Jr., and J. L. Pritchard, *J. Appl. Phys.* **37**, 1551 (1966).
- ³³R. D. Levine and R. B. Bernstein, *Molecular Reaction Dynamics* (Oxford University, New York, 1974).
- ³⁴P. J. Kuntz, in *Dynamics of Molecular Collisions, Part B*, edited by W. H. Miller (Plenum, New York, 1976), pp. 53–120.
- ³⁵C. A. Parr, Ph.D. thesis, California Institute of Technology, 1969.
- ³⁶For a general discussion of geometries in H_2X systems, see M. M. L. Chen and H. F. Schaefer III, *J. Chem. Phys.* **72**, 4376 (1980).
- ³⁷J. C. Polanyi and J. L. Schreiber, in *Physical Chemistry, An Advanced Treatise*, Vol. VI A of *Kinetics of Gas Reactions*, edited by W. Jost (Academic, New York, 1974), Chap. 6.
- ³⁸(a) S. A. Pace and J. M. White, *Int. J. Chem. Kinet.* **7**, 951 (1975); (b) J. M. White, *J. Chem. Phys.* **65**, 3674 (1976).
- ³⁹B. E. Holmes and D. W. Setser, in *Physical Chemistry of Fast Reactions*, Vol. 2 of *Reaction Dynamics*, edited by I. W. M. Smith (Plenum, New York, 1980), Chap. 2, p. 83.
- ⁴⁰A. M. G. Ding, L. J. Kirsch, D. S. Perry, J. C. Polanyi, and D. L. Schreider, *Faraday Discuss. Chem. Soc.* **55**, 252 (1973); J. C. Polanyi, J. J. Sloan, and J. Wanner, *Chem. Phys.* **13**, 1 (1976); J. C. Polanyi and J. L. Schreiber, *Faraday Discuss. Chem. Soc.* **62**, 267 (1977); J. C. Polanyi and N. Sathyamurthy, *Chem. Phys.* **37**, 259 (1979).
- ⁴¹J. M. White, *J. Chem. Phys.* **58**, 4482 (1973).
- ⁴²(a) P. Botschwina and W. Meyer, *J. Chem. Phys.* **67**, 2390 (1977); (b) T. H. Dunning and co-workers found a barrier to abstraction of 15 kcal/mol for HBr (private communication).
- ⁴³(a) W. Bauer, L. Y. Rusin, J. P. Toennies, and K. Walschewski, *J. Chem. Phys.* **66**, 3837 (1977); (b) U.

- Schwalm and J. P. Toennies, *Chem. Phys. Lett.* **63**, 17 (1979);
- ⁴⁴J. W. Hepburn, D. Klimek, K. Liu, R. G. Macdonald, H. R. Mayne, F. J. Northrup, and J. C. Polanyi, *Int. J. Chem. Kinet.*, Laidler Festschrift (to be published).
- ⁴⁵D. S. Perry and J. C. Polanyi, *Chem. Phys.* **12**, 37 (1976).
- ⁴⁶H. S. Johnston, *Gas Phase Reaction Rate Theory* (Ronald, New York, 1966), pp. 209ff, 339ff.
- ⁴⁷G. A. Takacs and G. P. Glass, *J. Phys. Chem.* **77**, 1060 (1973).
- ⁴⁸M. A. Eliason and J. O. Hirschfelder, *J. Chem. Phys.* **30**, 1426 (1959).
- ⁴⁹B. A. Blackwell, J. C. Polanyi, and J. J. Sloan, *Chem. Phys.* **30**, 299 (1978).
- ⁵⁰H. H. Dispert, M. W. Geis, and P. R. Brooks, *J. Chem. Phys.* **70**, 5317 (1979).